Arabian Journal for Science and Engineering (2019) 44:579–589
https://doi.org/10.1007/s13369-018-3485-7

RESEARCH ARTICLE - PHYSICS

Interpretation of Chemical Reactions and Activation Energy for Unsteady 3D Flow of Eyring–Powell Magneto-Nanofluid

A. S. Alshomrani[1] · M. Zaka Ullah[1] · S. S. Capizzano[2] · W. A. Khan[3] · M. Khan[4]

Received: 22 December 2017 / Accepted: 25 July 2018 / Published online: 10 August 2018

Abstract
Refrigeration of electronic instruments, in view of environmental concern and energy security, is one of the main challenges of the new generation technology. The miniaturization of electronic devices has benefits, but in such situations, the heat dissipated per unit area rises in an uncontrolled manner. This can be done by either improving the characteristics of secondary and primary working liquids or by modifying the system. In this article, we present a comprehensive detail of unsteady 3D flow of Eyring–Powell nanofluid with convective heat and mass flux conditions. The effects of heat source–sink and nonlinear thermal radiations are considered in the Eyring–Powell nanofluid model. Additionally, chemical mechanism responsible for the mass transfer such as activation energy is accounted in the current relation. Moreover, suitable transformations are betrothed to obtain coupled nonlinear ordinary differential equations (ODEs) from the system of highly nonlinear coupled partial differential equations and numerical solution of system of coupled ODEs is obtained by means of bvp4c scheme. Our findings demonstrate that heat flux at the wall declines by uplifting the chemical reaction rate constant. The concentration of Eyring–Powell nanofluid is directly affected by activation energy of chemical process, and a trend of thermophoretic force on magneto-nanofluid is qualitative, contradictory to that of Brownian motion.

Keywords Unsteady 3D flow · Eyring–Powell model · Nanoparticles · Nonlinear thermal radiation · New mass flux boundary conditions

Nomenclature

u, v, w	Velocity components
x, y, z	Space coordinates
v	Kinematics viscosity
β, d_1	Liquid parameters
m	Fitted rate constant
$(\rho c)_f$	Heat capacity of fluid
T	Temperature of fluid
k	Thermal conductivity
α_1	Thermal diffusivity
τ	Effective heat capacity ratio
D_B	Brownian diffusion coefficient
D_T	Thermophoresis diffusion coefficient
T_∞	Ambient fluid temperature
C	Nanoparticles concentration
Q_0	Heat generation/absorption parameter
C_∞	Ambient nanoliquid concentration
E_a	Activation energy
t	Time
h_t	Wall heat transfer coefficients
a, b	Positive constants
σ^*	Stefan–Boltzmann constant
k^*	Mean absorption coefficient
β_1	Dimensional unsteadiness parameter
$U_w(x,t), V_w(x,t)$	Stretching velocities
q_r	Radiative heat flux
k_c	Rate of chemical reaction
C_c	Concentration of the heated fluid
h_c	Mass transfer coefficient
K	Boltzmann constant
η	Dimensionless variable

✉ A. S. Alshomrani
aszalshomrani@kau.edu.sa

[1] NAAM Research Group, Department of Mathematics, Faculty of Science, King Abdulaziz University, Jeddah 21589, Saudi Arabia

[2] Department of Science and High Technology, University of Insubria, Via Valleggio 11, 22100 Como, Italy

[3] Department of Mathematics and Statistics, Hazara University, Mansehra 21300, Pakistan

[4] Department of Mathematics, Quaid-i-Azam University, Islamabad 44000, Pakistan

$\varepsilon, \delta_1, \delta_2$	s The Eyring–Powell fluid parameters
S	Unsteadiness parameter
Pr	Prandtl number
$\lambda > 0$	Heat generation parameter
$\lambda < 0$	Heat absorption parameter
N_{b}	Brownian motion parameter
N_{t}	Thermophoresis parameter
R_d	Radiation parameter
Le	Lewis number
α	Ratio of stretching rates parameter
M	Magnetic parameter
γ	Thermal Biot number
γ_1	Concentration Biot number
σ	Chemical reaction parameter
δ	Temperature difference parameter
θ_f	Temperature ratio parameter
E	Activation energy parameter
f, g	Dimensionless velocities
θ	Dimensionless temperature
ϕ	Dimensionless concentration
Nu_x	Local Nusselt number
Re_x	Local Reynolds number
Sh_x	Local Sherwood number

1 Introduction

In the age of nanotechnology and nanoscience advancement, the effectiveness and efficiency of industrial applications are becoming more prominent. Continuous developments are essential to sustain the nanotechnology. Nanotechnologies are overhauled persistently by adopting innovative concepts. Nanoscience is the liveliest area of research that fascinates investigators because of its higher potential, enabling a substantial improvement in the performance of numerous electrical devices. Investigators have considered nanoparticles of various metals, oxides of metals, nitrides, carbides and numerous types of carbon with various base liquids. Nanoliquids are prepared by adopting two-step and one-step methods. Foremost purpose of adopting these techniques is to prepare stable and homogenous mixtures to avoid the possible erosion, agglomeration and clogging. In one-step technique, nanoparticles are made first and then these particles are dispersed into base liquid while in the two-step technique, nanoparticles are produced in first step and then these particles are dispersed into a host liquid in the second step. Recently, nanoliquids have received meticulous attention in heat transfer mechanism because of their promising performance as cooling and heating liquids. Heat dissipation in electronic devices has become a significant factor in the electronic instruments' designing. It is observed that by utilizing nanoliquids in thermosiphons and heat pipes, one can enhance the rate of heat transfer mechanism from one point to another. The concept of nanoliquid was initially conceived by Choi et al. [1], which intended to rise the rate of the heat transfer. Oztop and Abu-Nada [2] addressed the natural convective flow of partially heated surfaces by utilizing the nanoparticles aspects. Khan et al. [3] developed the mathematical relation for 3D flow of an Oldroyd-B fluid by considering the aspects of nanoparticles and utilizing the heat source–sink mechanisms. Sheikholeslami and Ellahi [4] studied the 3D flow of natural convective flow of magneto-nanofluid by utilizing the cubic cavity. Akbar et al. [5] examined the characteristics of induced MHD on carbon nanotubes in peristaltic flow. Sandeep et al. [6] investigated the impact of convective heat–mass transfer mechanisms on non-Newtonian magneto-nanofluid. Rehman et al. [7] considered the aspect of entropy generation for nanofluids by utilizing the revised and more realistic relation for the nanofluid. Haq et al. [8] investigated the impact of H_2O- and $C_2H_6O_2$-based Cu nanoparticles by utilizing two parallel disks. Rahman et al. [9] investigated the impact of slip on a non-Newtonian fluid with nanoparticles in tapered artery with stenosis. Hayat et al. [10] provided the characteristics of chemical processes for nanofluid utilizing the rotating disk. Hayat et al. [11] inspected the characteristics of magneto-nanofluid by making use of the variable rotating disk. Sandeep [12] deliberated the impact of aligned MHD on nanofluid by utilizing a thin film.

In any chemical process, mass transfer mechanism is mainly dependent upon the species whose concentration is varied. In these situations, movement of species is detected from region of low concentration to an area of high concentration. Chemical process is an essential part of innovations, of cultures and, in fact, of life itself. There are different types of chemical reactions; some of them are proceeded through reaction mechanisms, while others through just a mechanism. Most of them are complex in nature which consist of a number of chemical reaction steps, also known as the elementary steps. Mass–heat transfer mechanism via chemical processes has been an area of concern for investigators because of its huge applications like geothermal reservoirs, cooling of nuclear reactor and recovery of thermal oil. Generally, the reactions are divided into two types: the homogeneous reactions and heterogeneous reactions. The reaction in which the involved species are in the same state/phase, e.g., gas–gas phase/state or liquid–liquid phase/state, is a homogeneous reaction, while in a heterogeneous reaction, the involved species are from different phase spaces. The term activation energy has a significant part in chemical reactions. Arrhenius presented the idea of activation energy in 1889 for the first time. It is the least required amount of energy for the species that change the reactants into products. Activation energy can be in the form of potential energy or kinetic energy. In the absence of activation energy, reactants cannot form the products; conversely, a reaction occurs when the movement of the particles is rapid due to activation energy.

The applications of activation energy are varied in chemical engineering, geothermal and mechanics of water and oil emulsions. Ramzan et al. [13] presented the mathematical relation to examine the impact of binary reaction and activation energy on the magneto-nanofluid. Ramzan et al. [14] studied the characteristics of chemical process and double stratification on radiative flow of Powell–Eyring magneto-nanofluid. Shafique et al. [15] investigated the aspects of activation energy and rotating frame on the Maxwell fluid flow. Khan et al. [16] analyzed the effect of chemical process on the 3D flow of Burgers fluid. Khan et al. [17] inspected the impact of chemical reaction on generalized Burgers fluid by utilizing the nanoparticles. Mustafa et al. [18] examined the characteristics of activation energy and chemical mechanism on the magneto-nanofluid.

In the advanced life of today, energy is one of the major necessities that facilitates economic growth in societies. There are numerous types of sources of energy, such as wind energy, thermal energy, solar energy, and biomass energy. The investigators believe that among these sources of energy, solar energy is the best replacement of energy sources. Solar energy is a mechanism in which energy spreads from a heated surface to its absorption point in all directions in the form of electromagnetic waves. It is generated by the thermal agitation of composite molecules of a body. Furthermore, the latest development in science and technology is much indebted to solar energy due to its massive utilization in solar heating, solar photovoltaic cells, solar thermal electricity and artificial photosynthesis. By keeping these applications of solar energy in mind, we have deliberated the aspects of radiation. Khan et al. [19] considered the aspects of gyrotactic microorganisms for Magneto–Burgers nanofluid in the presence of thermal radiation. Ali et al. [20] studied the hidden mechanism for unsteady flow by utilizing porous medium. Bhatti et al. [21] investigated the heat transfer mechanism for MHD particle–fluid suspension under the influence of thermal radiation induced by metachronal wave. Khan et al. [22] used the idea of suspension of nanoparticles into 3D Sisko fluid flow over stretched surface.

From the abovementioned debate, it has provided the idea for the application of nanofluids to make a novel extrusion manufacturing process of thermal system, and to produce highly effective devices to promote the manufacturing economic efficiency. Additionally, it is gathered from the above discussion that current consideration is unique, and no such investigation has been considered in the literature before. Therefore, the main theme of this research article is to investigate the characteristics of thermal energy extrusion system for unsteady 3D flow of Eyring–Powell nanofluid with radiation and heat source–sink aspects. Moreover, the novelty of this research work is that it provides a novel activation energy on Eyring–Powell nanofluid aspect on thermal extrusion energy system. The features of activation energy for magneto-Eyring–Powell nanofluid are controlled by some significant physical parameters.

2 Methodology

2.1 Theory and Analysis

Figure 1 presents the physical model for unsteady 3D forced convective flow of an electrically conducting Eyring–Powell nanofluid over a bidirectional stretching surface. The sheet is stretched along $x-$ and $y-$ directions with velocities $u = U_w(x,t) = \frac{ax}{1-\beta_1 t}$ and $v = V_w(y,t) = \frac{by}{1-\beta_1 t}$, respectively, in which $a, b > 0$ are constants. Furthermore, we assume that heated fluid under the sheet with temperature T_t is used to change the temperature of the sheet by convective heat transfer mode, which provides us the heat transfer coefficient h_t. Convectively heated surface can be utilized for numerous industrial products, such as food sheet, metal sheet and plastic sheet. The current design presents a device for finding an excellent efficiency thermal energy conversion manufacturing process. Because liquid below the bidirec-

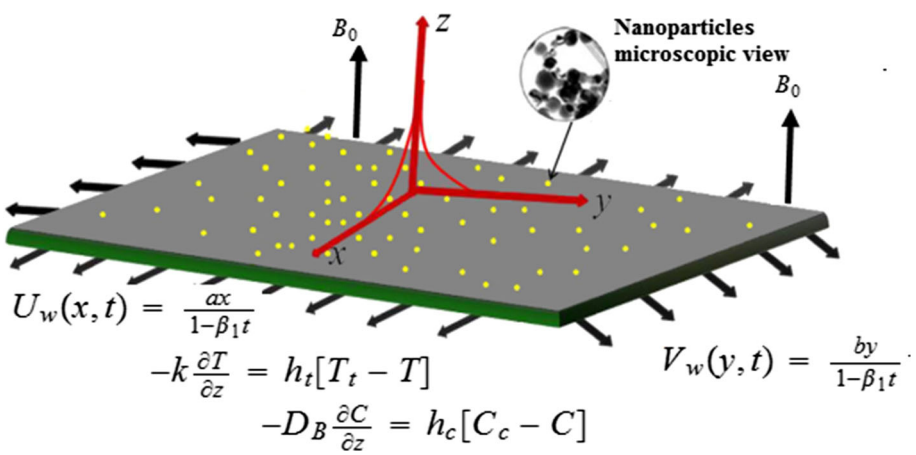

Fig. 1 The physical geometry for the problem

tional sheet is hot and needed to be cooled by the working liquid; therefore, an excellent liquid flow was selected to do this job. Moreover, to achieve a good impact, activation energy has been utilized. In this article, many useful factors have been considered which improve the manufacturing process. The related physical theory has been introduced in the following section.

2.1.1 Fluid Field Analysis

Here, the unsteady 3D forced convective flow of an electrically conducting non-Newtonian fluid, namely Eyring–Powell nanofluid associated with convective heat and mass transfer, has been considered. The sheet coincides with the plane $z = 0$, and motion of Eyring–Powell nanofluid is confined in the half space $z > 0$. Constructive–destructive chemical reactions, activation energy and heat source–sink mechanisms are also taken into account. Additionally, Reynolds number is supposed to be small neglecting the impact of induced magnetic field on the Eyring–Powell nanofluid. The nanofluid outside the boundary is maintained at a uniform temperature and concentration, (T_∞, C_∞), respectively. In areas such as geothermal, the governing equations are:

$$\frac{\partial u}{\partial x}+\frac{\partial v}{\partial y}+\frac{\partial w}{\partial z}=0, \tag{1}$$

$$\frac{\partial u}{\partial t}+u\frac{\partial u}{\partial x}+v\frac{\partial u}{\partial y}+w\frac{\partial u}{\partial z}=\left(\nu+\frac{1}{\beta d_1\rho_{\mathrm{f}}}\right)\frac{\partial^2 u}{\partial z^2} -\frac{1}{2\beta d_1^3\rho_{\mathrm{f}}}\left(\frac{\partial u}{\partial z}\right)^2\frac{\partial^2 u}{\partial z^2}-\frac{\sigma B_0^2(t)}{\rho_{\mathrm{f}}}u, \tag{2}$$

$$\frac{\partial v}{\partial t}+u\frac{\partial v}{\partial x}+v\frac{\partial v}{\partial y}+w\frac{\partial v}{\partial z}=\left(\nu+\frac{1}{\beta d_1\rho_{\mathrm{f}}}\right)\frac{\partial^2 v}{\partial z^2} -\frac{1}{2\beta d_1^3\rho_{\mathrm{f}}}\left(\frac{\partial v}{\partial z}\right)^2\frac{\partial^2 v}{\partial z^2}-\frac{\sigma B_0^2(t)}{\rho_{\mathrm{f}}}v, \tag{3}$$

$$\frac{\partial T}{\partial t}+u\frac{\partial T}{\partial x}+v\frac{\partial T}{\partial y}+w\frac{\partial T}{\partial z} =\alpha_1\frac{\partial^2 T}{\partial z^2}+\tau\left[D_{\mathrm{B}}\frac{\partial C}{\partial z}\frac{\partial T}{\partial z}+\frac{D_{\mathrm{T}}}{T_\infty}\left(\frac{\partial T}{\partial z}\right)^2\right] -\frac{1}{(\rho c)_{\mathrm{f}}}\frac{\partial q_{\mathrm{r}}}{\partial z}+\frac{Q_0}{(\rho c)_{\mathrm{f}}}(T-T_\infty), \tag{4}$$

$$\frac{\partial C}{\partial t}+u\frac{\partial C}{\partial x}+v\frac{\partial C}{\partial y}+w\frac{\partial C}{\partial z}=D_{\mathrm{B}}\frac{\partial^2 C}{\partial z^2} -k_{\mathrm{c}}^2(C-C_\infty)\left(\frac{T}{T_\infty}\right)^m\exp\left(-\frac{E_{\mathrm{a}}}{KT}\right)+\frac{D_{\mathrm{T}}}{T_\infty}\frac{\partial^2 T}{\partial z^2}. \tag{5}$$

The boundary conditions for the present flow analysis are:

$$u=U_w(x,t)=\frac{ax}{1-\beta_1 t},\ v=V_w(y,t)=\frac{by}{1-\beta_1 t},\ w=0,$$

$$-k\frac{\partial T}{\partial z}=h_{\mathrm{t}}[T_{\mathrm{t}}-T],-D_{\mathrm{B}}\frac{\partial C}{\partial z}=h_{\mathrm{c}}[C_{\mathrm{c}}-C]\ \text{at}\ z=0, \tag{6}$$

$$u\to 0,\ v\to 0,\ T\to T_\infty,\ C\to C_\infty\ \text{as}\ z\to\infty. \tag{7}$$

The radiative heat flux q_{r} is given by:

$$q_{\mathrm{r}}=-\frac{4\sigma^*}{3k^*}\frac{\partial T^4}{\partial z}=-\frac{16\sigma^*}{3k^*}T^3\frac{\partial T}{\partial z}. \tag{8}$$

Substituting Eqs. (8) into (4), we have the following energy equation

$$\frac{\partial T}{\partial t}+u\frac{\partial T}{\partial x}+v\frac{\partial T}{\partial y}+w\frac{\partial T}{\partial z} =\alpha_1\frac{\partial^2 T}{\partial z^2}+\tau\left[D_{\mathrm{B}}\frac{\partial C}{\partial z}\frac{\partial T}{\partial z}+\frac{D_{\mathrm{T}}}{T_\infty}\left(\frac{\partial T}{\partial z}\right)^2\right] +\frac{1}{(\rho c)_{\mathrm{f}}}\frac{16\sigma^*}{3k^*}\frac{\partial}{\partial z}\left(T^3\frac{\partial T}{\partial z}\right)+\frac{Q_0}{(\rho c)_{\mathrm{f}}}(T-T_\infty). \tag{9}$$

Via presenting the following suitable conversions,

$$u=\frac{axf'(\eta)}{1-\beta_1 t},\ v=\frac{ayg'(\eta)}{1-\beta_1 t},\ w=-\sqrt{\frac{a\nu}{1-\beta_1 t}}\,[f(\eta)+g(\eta)],$$
$$\theta(\eta)=\frac{T-T_\infty}{T_{\mathrm{t}}-T_\infty},\ \varphi(\eta)=\frac{C-C_\infty}{C_{\mathrm{c}}-C_\infty},\ \eta=z\sqrt{\frac{a}{\nu(1-\beta_1 t)}}. \tag{10}$$

Equation (1) is automatically satisfied, and Eqs. (2)–(7) and (9) yield

$$(1+\varepsilon)f'''-S\left(f'+\frac{1}{2}\eta f''\right)+(f+g)f''-f'^2 -\varepsilon\delta_1 f''^2 f'''-M^2 f'=0, \tag{11}$$

$$(1+\varepsilon)g'''-S\left(g'+\frac{1}{2}\eta g''\right)+(f+g)g''-g'^2 -\varepsilon\delta_2 g''^2 g'''-M^2 g'=0, \tag{12}$$

$$\frac{d}{d\eta}\left[\left\{1+R_d\left(1+(\theta_f-1)\theta\right)^3\right\}\theta'\right]-\Pr S\left(\theta+\frac{1}{2}\eta\theta'\right) +\Pr[(f+g)\theta'+N_{\mathrm{b}}\theta'\varphi'+N_{\mathrm{t}}\theta'^2]+\Pr\lambda\theta=0, \tag{13}$$

$$\varphi''-\frac{1}{2}Le\Pr S\eta\varphi'+Le\Pr(f+g)\varphi'-Le\Pr\sigma(1+\delta\theta)^m \exp\left(-\frac{E}{1+\delta\theta}\right)+\frac{N_{\mathrm{t}}}{N_{\mathrm{b}}}\theta''=0, \tag{14}$$

$$f=0,\ \ g=0,\ \ \ f'=1,\ \ g'=\alpha,$$
$$\theta'(0)=-\gamma[1-\theta(0)],\ \ \varphi'(0)=-\gamma_1[1-\varphi(0)],$$
$$at\ \ \eta=0, \tag{15}$$

$$f'\to 0,\ g'\to 0,\ \theta\to 0,\ \varphi\to 0,\ \text{as}\ \eta\to\infty. \tag{16}$$

In the above expressions, $(\varepsilon, \delta_1, \delta_2, M, \alpha, \gamma, \gamma_1, R_d, \theta_f, Pr, N_b, N_t, \lambda, Le, \sigma, \delta, E)$ are, respectively, the Eyring–Powell fluid parameters, magnetic parameter, ratio of stretching rates parameter, thermal Biot number, concentration Biot number, radiation parameter, temperature ratio parameter, Prandtl number, Brownian motion parameter, thermophoresis parameter, heat source-sink parameter, Lewis number, chemical reaction parameter, temperature difference parameter and activation energy parameter. Mathematically these parameters are expressed in the following manner:

$$\varepsilon = \left(\frac{1}{\beta d_1 \rho_f}\right), \delta_1 = \left(\frac{a^3 x^2}{2\nu d_1^2}\right), \delta_2 = \left(\frac{a^3 y^2}{2\nu d_1^2}\right),$$
$$R_d = \frac{16\sigma^* T_\infty^3}{3kk^*},$$
$$M^2 = \frac{\sigma B_0^2(1-\beta_1 t)}{(\rho a)_f}, N_b = \frac{\tau D_B (C_c - C_\infty)}{\nu},$$
$$N_t = \frac{\tau D_T (T_t - T_\infty)}{\nu T_\infty}, \lambda = \frac{Q_0(1-\beta_1 t)}{a(\rho c)_f}, \alpha = \frac{b}{a},$$
$$Pr = \frac{\nu}{\alpha_1}, Le = \frac{\alpha_1}{D_B}, \sigma = \frac{k_c^2}{a}, E = \frac{E_a}{KT}, \delta = \frac{T_f - T_\infty}{T_\infty},$$
$$\theta_f = \frac{T_f}{T_\infty}. \quad (17)$$

2.1.2 Heat–Mass Transfer Analysis

Chemical and physical quantities of interest in this research work are the rate of heat–mass transfer which are given through Fourier and Fick's relations as follows:

$$Nu_x = -\frac{x}{(T_t - T_\infty)}\left(\frac{\partial T}{\partial z}\right)\Big|_{z=0} + \frac{x q_r}{k(T_t - T_\infty)},$$
$$Sh_x = -\frac{x}{(C_c - C_\infty)}\left(\frac{\partial C}{\partial z}\right)\Big|_{z=0}. \quad (18)$$

The above quantities are reduced in the following dimensionless form:

$$(Re_x)^{-\frac{1}{2}} Nu_x = -\left[1 + \frac{4}{3}R_d\{\theta_f + (1-\theta_f)\theta\}^3\right]\theta'(0),$$
$$(Re_x)^{-\frac{1}{2}} Sh_x = -\varphi'(0), \quad (19)$$

where $Re_x = \frac{ax^2}{\nu}$ is the local Reynolds number.

2.1.3 Numerical Technique

The transformed ODEs, i.e., Eqs. (11)–(14), are highly nonlinear, and exact solutions of these equations, in general, look almost impossible. Consequently, we implement the numerical technique, namely bvp4c scheme to construct the solutions of these equations. In this technique, we reduce the coupled ODEs into first-order differential equations and convert them into a set of IVP. These initial value problems (IVPs) are then solved by setting some initial guesses for three unknown initial conditions. To achieve this objective, we modify Eqs. (11)–(16) into first-order differential structures as follows:

$$f = y_1,\ f' = y_2,\ f'' = y_3,\ f''' = yy_1, \quad (20)$$
$$g = y_4,\ g' = y_5,\ g'' = y_6,\ g''' = yy_2, \quad (21)$$
$$\theta = y_7,\ \theta' = y_8,\ \theta'' = yy_3, \quad (22)$$
$$\varphi = y_9,\ \varphi' = y_{10},\ \varphi'' = yy_4, \quad (23)$$
$$yy_1 = \frac{S\left(y_2 + \frac{1}{2}\eta y_3\right) - (y_1 + y_4)y_3 + y_2^2 + M^2 y_2}{A_1},$$
$$A_1 = \left(1 + \varepsilon - \varepsilon\delta_1 y_3^2\right) \quad (24)$$
$$yy_2 = \frac{S\left(y_5 + \frac{1}{2}\eta y_6\right) - (y_1 + y_4)y_6 + y_5^2 + M^2 y_5}{A_2},$$
$$A_2 = \left(1 + \varepsilon - \varepsilon\delta_2 y_6^2\right), \quad (25)$$

$$yy_3 = \frac{-Pr[(y_1 + y_4)y_8 + N_b y_8 y_{10} + N_t y_8^2 + \lambda y_7] - 3R_d(1 + (\theta_f - 1)y_7)^2((\theta_f - 1)y_8^2)}{A_3}$$
$$+ \frac{PrS\left(y_7 + \frac{1}{2}\eta y_8\right)}{A_3}, \quad (26)$$

$$A_3 = \left(1 + R_d(1 + (\theta_f - 1)y_7)^3\right), \quad (27)$$
$$yy_4 = \frac{1}{2}Le\,\mathrm{Pr}S\eta y_{10} - Le\,\mathrm{Pr}(y_1 + y_4)y_9$$
$$+ Le\,\mathrm{Pr}\,\sigma(1 + \delta y_7)^m \exp\left(-\frac{E}{1 + \delta y_7}\right) - \frac{N_t}{N_b}yy_3, \quad (28)$$
$$y_1(0) = 0,\ y_2(0) = 1,\ y_2(\infty) = 0, \quad (29)$$
$$y_4(0) = 0,\ y_5(0) = \alpha,\ y_5(\infty) = 0, \quad (30)$$
$$y_8(0) + \gamma(1 - y_7(0)) = 0,\ y_7(\infty) = 0, \quad (31)$$
$$y_{10}(0) + \gamma_1(1 - y_9(0)) = 0,\ y_9(\infty) = 0, \quad (32)$$

3 Results and Discussion

This section focuses on the physical explanation of involved parameters of heat and mass transfer distributions. Heat source–sink and nonlinear radiation effects are taken into consideration. The governing ODEs and boundary condi-

Table 1 Numerical values of $(Re_x)^{-\frac{1}{2}} Nu_x$ for distinct values of escalating parameters when $\varepsilon = 0.3, \delta_1 = \delta_2 = 0.2, M = 0.5, m = 0.8, \alpha = 0.3, Le = 1.0, \gamma = 0.2, R_d = 0.5, \theta_f = 0.3, \lambda = 0.1$ and $\delta = 1$

N_t	N_b	Pr	γ_1	E	σ	m	$(Re_x)^{\frac{-1}{2}} Nu_x$
0.1	0.1	0.1	0.5	1.0	1.0	0.8	0.173448
0.5	–	–	–	–	–	–	0.147829
0.8	–	–	–	–	–	–	0.1254
–	0.3	-	-	-	-	-	0.12055
–	0.6	-	-	-	-	-	0.113466
–	0.9	–	–	–	–	–	0.106611
–	–	1.1	–	–	–	–	0.137692
–	–	1.3	–	–	–	–	0.166928
–	–	1.7	–	–	–	–	0.224661
–	–	–	0.3	–	–	–	0.12146
–	–	–	0.6	–	–	–	0.128764
–	–	–	0.9	–	–	–	0.130583
–	–	–	–	0.0	–	–	0.129672
–	–	–	–	0.5	–	–	0.130117
–	–	–	–	0.9	–	–	0.130492
–	–	–	–	–	0.5	–	0.130962
–	–		–	–	0.8	–	0.130768
–	–	–	–	–	1.1	–	0.130493
–	–	–	–	–	–	0.2	0.130545
–	–	–	–	–	–	0.5	0.130571
–	–	–	–	–	–	0.9	0.130584

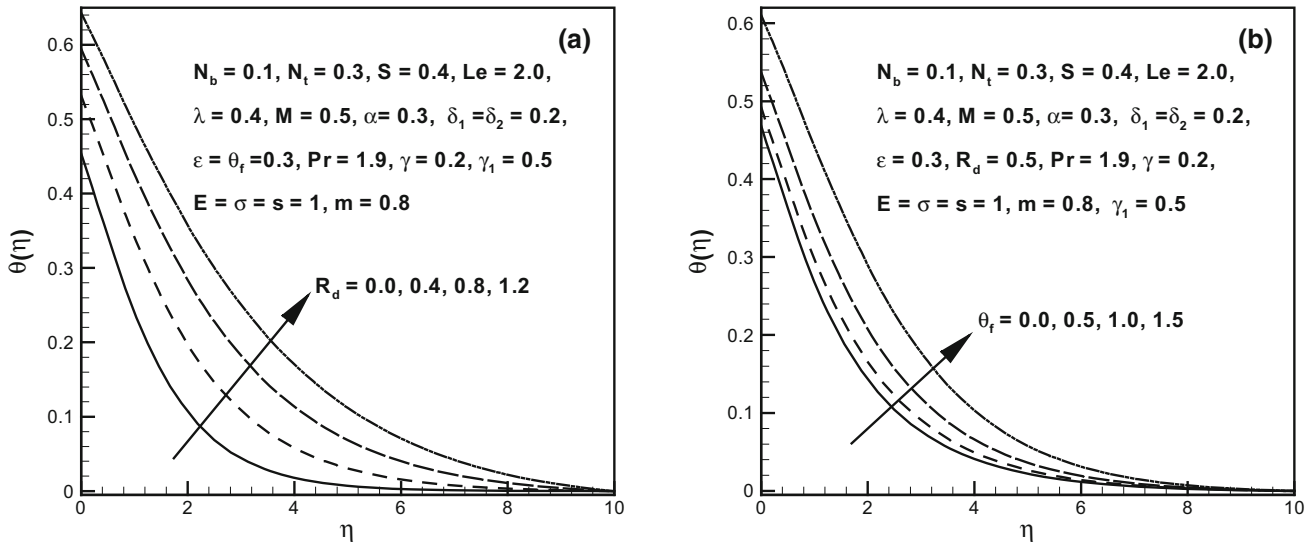

Fig. 2 **a**, **b** Profiles of temperature for various values of radiation parameter (panel a) and ratio of temperature ratio parameter (panel b)

tions are analyzed by utilizing bvp4c function in Matlab. A detailed graphical analysis has been made for the temperature and concentration fields. Additionally, heat transfer rate for fluctuating various parameters is included in Table 1. From Table 1, it is perceived that the heat transfer rate enriches for accumulative values of Pr, E, n and σ while it illustrates diminishing behavior for δ, m and N_t.

3.1 Temperature Field

The temperature profiles of Eyring–Powell nanofluid exhibits a remarkable change with the variation of R_d, θ_f, λ, Pr, N_b, N_t, γ and M. The variation of temperature profiles with these parameters is illustrated through Figs. 2, 3, 4 and 5. The influence of radiation parameter R_d and ratio of temperature ratio parameter θ_f on the temperature of Eyring–Powell

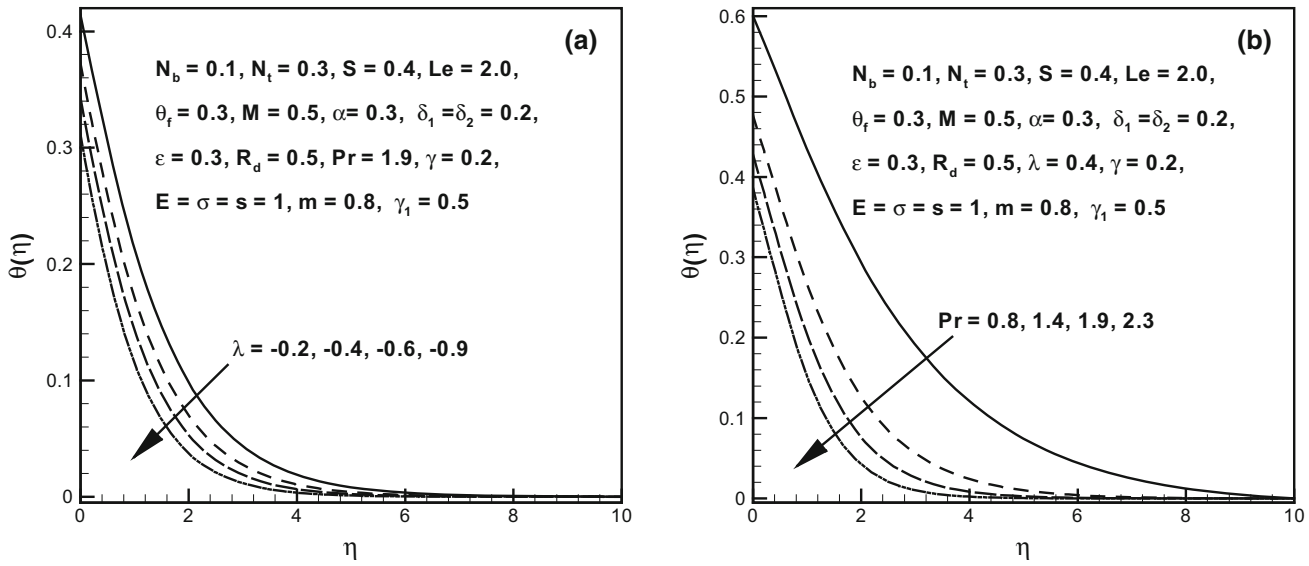

Fig. 3 **a**, **b** Profiles of temperature for various values of heat absorption parameter (panel a) and Prandtl number (panel b)

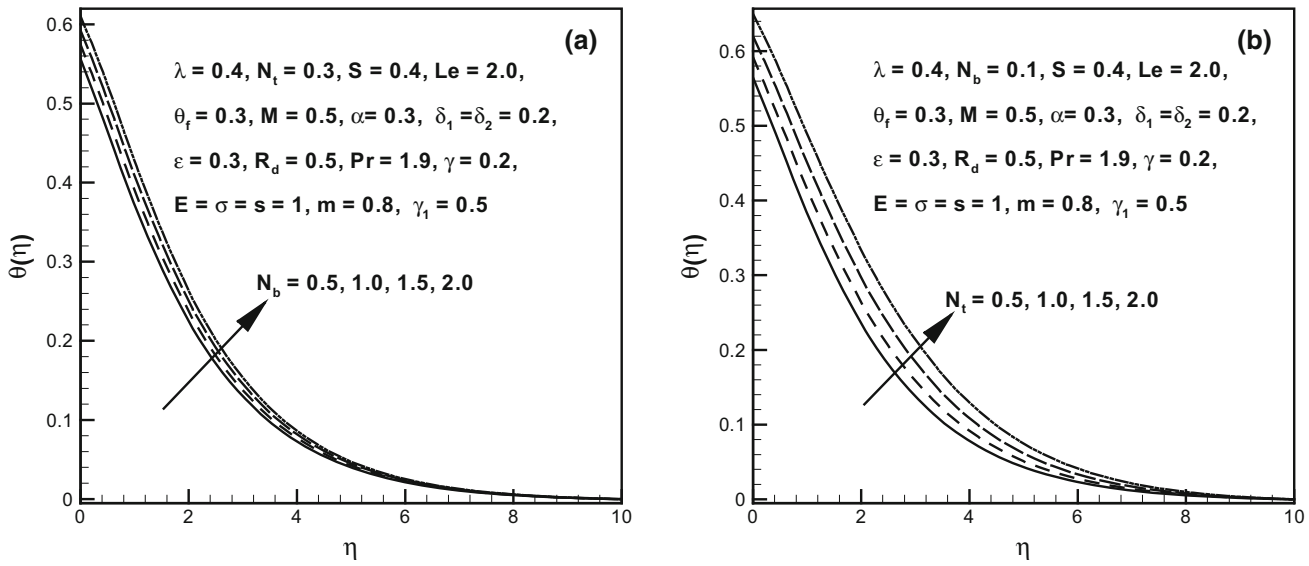

Fig. 4 **a**, **b** Profiles of temperature for various values of Brownian motion parameter (panel a) and thermophoresis parameter (panel b)

nanofluid is revealed in Fig. 2a, b. It is explored from these figures that the temperature profile augments with an increment in R_d and θ_f. From the mathematical point of view, R_d is directly proportional to temperature of nanoliquid at infinity. Consequently, as we augment R_d, the temperature of Eyring–Powell nanoliquid rises. Furthermore, as θ_f strengthens, the temperature of the wall becomes higher as compared to the temperature of nanoliquid at infinity. Thus, as a result, the temperature of nanofluid enhances.

Figure 3a, b presents the impact of heat absorption parameter λ and Prandtl number Pr on the temperature profile. These figures depict that the augmented values of θ_f and λ affect the heat transfer strongly. It is perceived from these sketches that deflating λ from -0.2 to -0.9 and inflating Pr from 0.8 to 2.3, the temperature of nanoliquid deteriorates. Figure 3b portrays that Pr affects the heat transfer processes strongly. Moreover, from the mathematical point of view, Pr has inverse relation with α_1. Therefore, as we rise Pr thermal diffusivity of nanoliquid drops, consequently, the temperature of nanoliquid decays.

The Brownian motion parameter N_b and thermophoresis parameter N_t play a vital role in forced convective 3D flow of Eyring–Powell nanofluid. Figure 4a, b is sketched to reveal the behavior of temperature of nanoliquid in response to change in N_b and N_t. It is perceived from these sketches that an increase in the temperature of nanoliquid is seen for

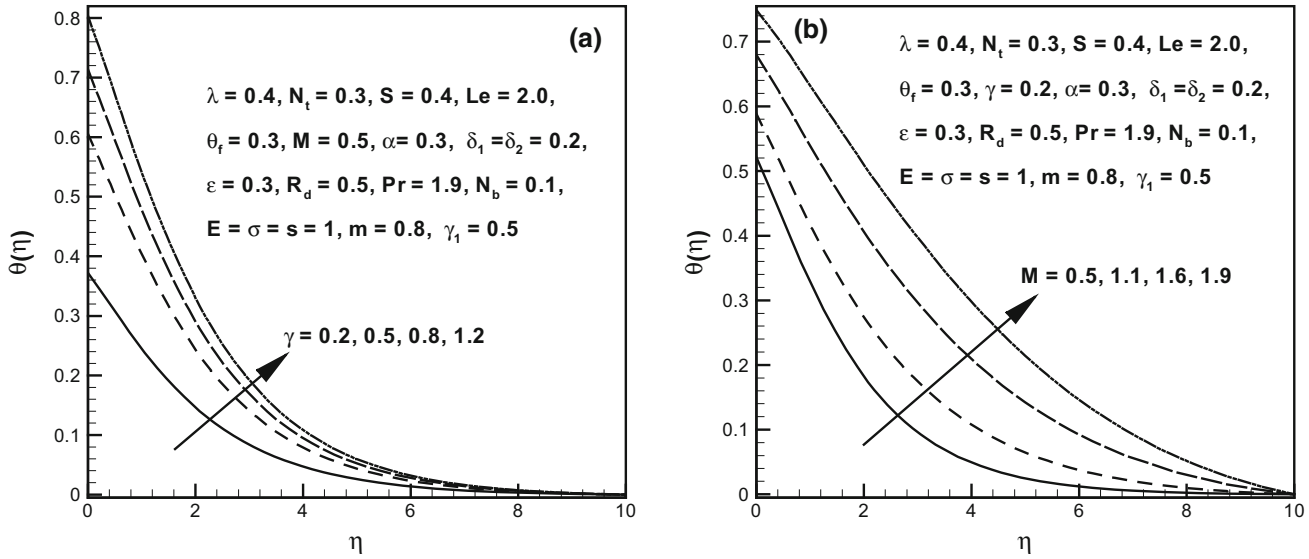

Fig. 5 **a**, **b** Profiles of temperature for various values of Biot number (panel a) and magnetic parameter (panel b)

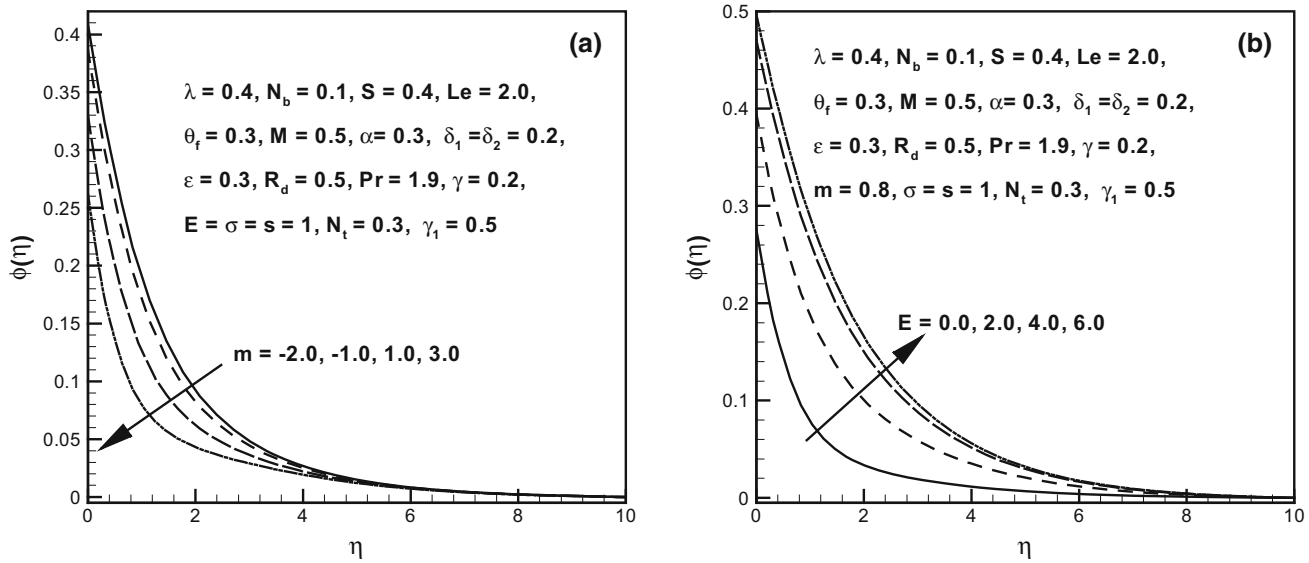

Fig. 6 **a**, **b** Profiles of concentration for various values of fitted rate constant (panel a) and activation energy parameter (panel b)

larger values of N_b, and N_t. Physically, N_b has direct relation with D_B. Larger N_b has higher D_B which enhances the temperature of nanoliquid. Additionally, an elevation in N_t leads to a boost-up in the thermophoretic force which tends to move the nanoliquid from a hotter to a colder region. Therefore, temperature of nanoliquid enhances.

Figure 5a, b interprets the dependence of the Biot number γ and magnetic parameter M on the temperature of nanofluid. The exploration of these plots imparts an enhancement in the temperature of the nanofluid. Physical reason behind this trend of γ is that less resistance is faced by the thermal wall which causes an enhancement in convective heat transfer to the fluid. Additionally, as we enhance M, Lorentz's force augments due to which collusion between the particles of Eyring–Powell nanofluid enhances. As a result, temperature of Eyring–Powell nanofluid rises.

3.2 Concentration Field

The influence of various parameters on the concentration of Eyring–Powell nanofluid is exhibited graphically through Figs. 6, 7, 8 and 9. Concentration profiles of Eyring–Powell nanofluid for different values of fitted rate constant m and activation energy parameter E are sketched through Fig 6a, b. The growing values of E result in an augmentation in the concentration of Eyring–Powell nanofluid while the reverse

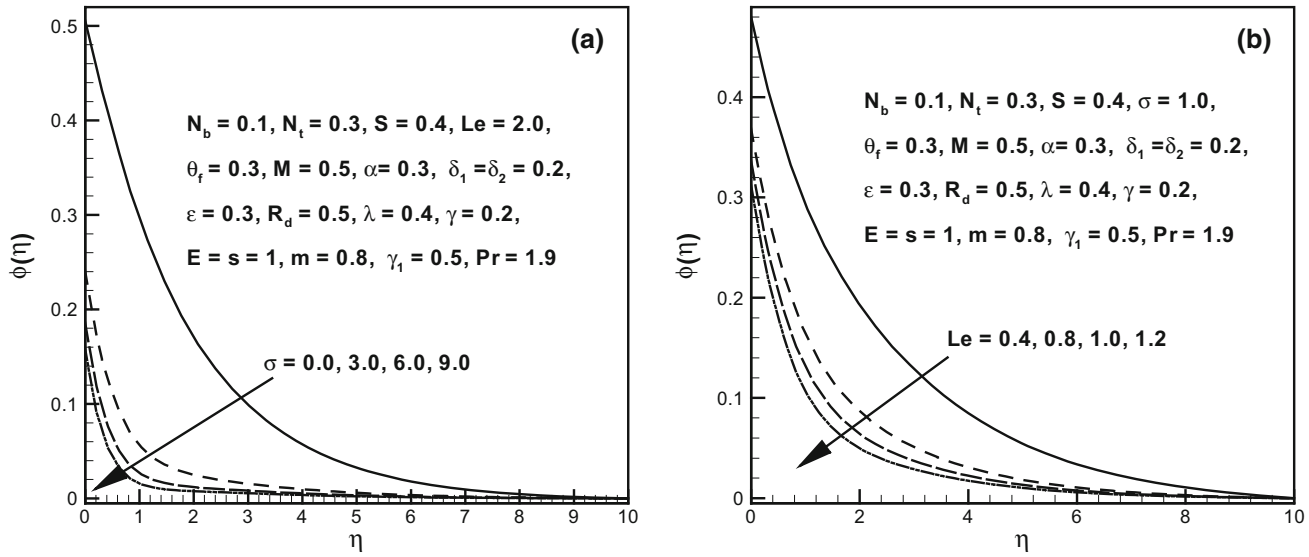

Fig. 7 **a**, **b** Profiles of concentration for various values of chemical reaction parameter (panel a) and Lewis number (panel b)

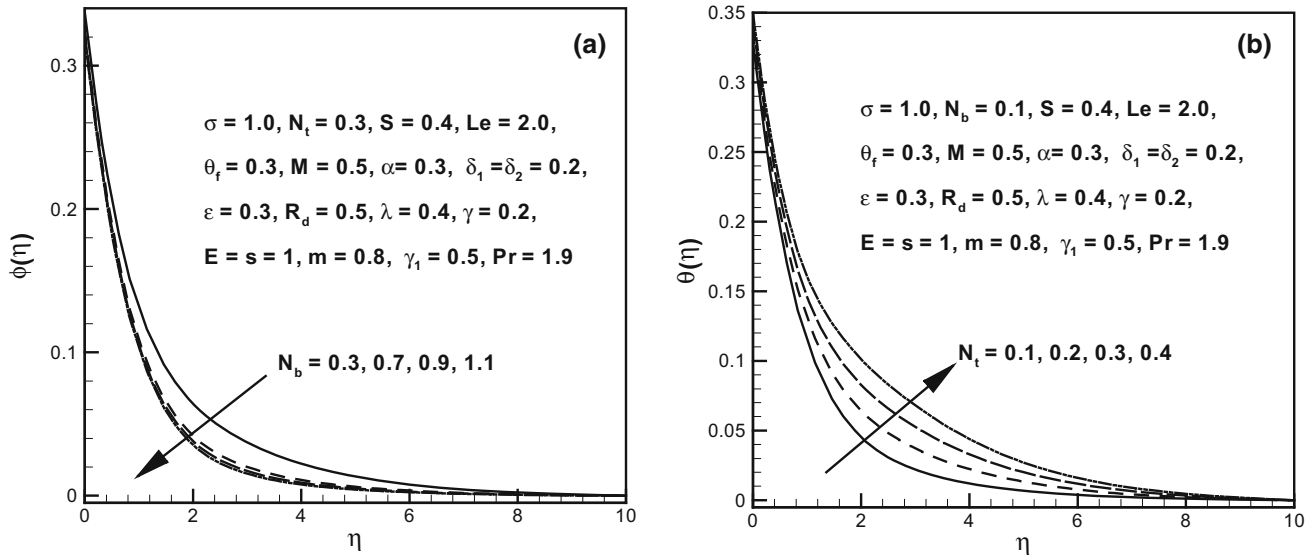

Fig. 8 **a**, **b** Profiles of concentration for various values of Brownian motion parameter (panel a) and thermophoresis parameter (panel b)

trend is detected for m. From the mathematical relation of equation (17), it is detected that high activation energy and low temperature reduces the reaction rate, due to which the chemical reaction mechanism slows down. Therefore, the concentration of Eyring–Powell nanofluid enhances. Additionally, as the values of m boost-up, destructive chemical mechanism enhances due to which concentration of Eyring–Powell nanofluid declines.

The influences of chemical reaction parameter σ and Lewis number Le on the concentration profile are displayed in Fig 7a, b. It is analyzed from these figures that the concentration profile declines with an increment in σ and Le.

Figure 8a, b portrays the concentration profile of Eyring–Powell nanofluid for various values of N_b, and N_t. It is detected from these sketches that concentration of Eyring–Powell nanofluid declines with elevation in N_t while the reverse trend is observed for N_b. Additionally, it is detected physically that an uplift in the magnitude of N_b corresponds to rise in the rate at which nanoparticles in the base liquid move in random directions with different velocities. This movement of nanoparticles augments transfer of heat and therefore declines the concentration profile.

To investigate the effects of the concentration Biot number γ_1 and Prandtl number Pr on the concentration profile, we have plotted Fig 9 a, b. These figures reveal that the concentration profile declines as the values of γ_1 and Pr are augmented.

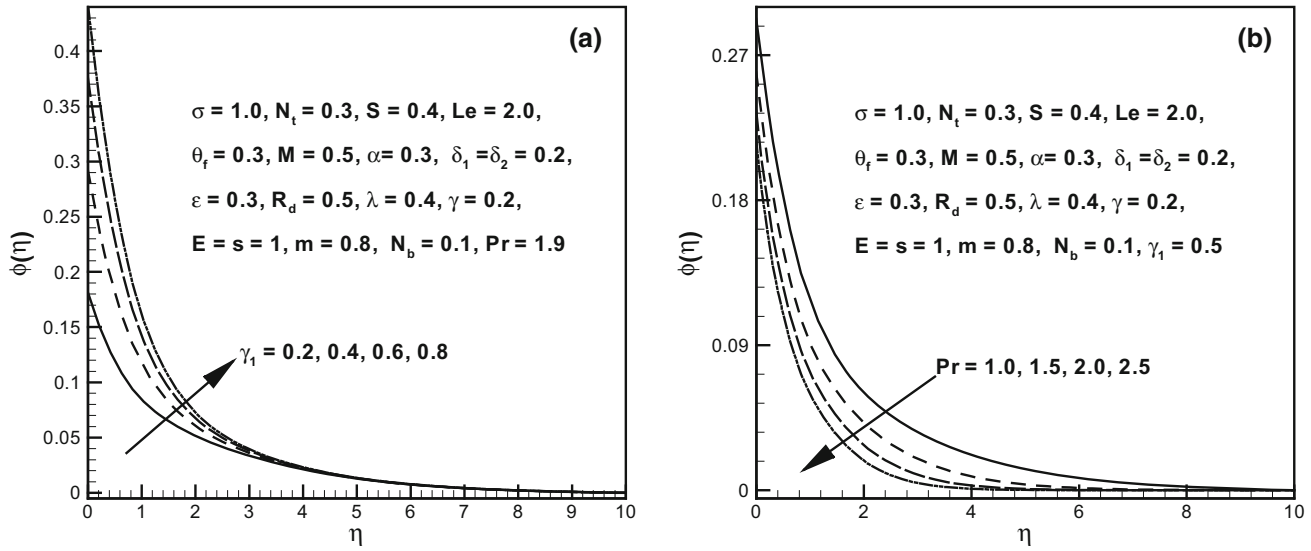

Fig. 9 **a**, **b** Profiles of concentration for various values of Biot number (panel a) and Prandtl number (panel b)

4 Conclusions

This article reports the unsteady 3D forced convective flow of an Eyring–Powell magneto-nanofluid under the impact of constructive–destructive reactions and inspects them numerically. Furthermore, the current thermal system was coupled with heat–mass transfer aspects and this thermal system was controlled for the cooling of electronic devices through important parameters to produce a high efficiency extrusion product by manufacturing process. The condition of activation energy was taken into account. The research problem was then solved numerically by using bvp4c scheme. The following observations are deduced from our graphical data and tables:

- The rising values of S and θ_f resulted in elevation of the liquid's temperature.
- Heat transfer rate improved for escalating activation energy parameter E.
- Heat flux at boundary diminished when thermophoresis effect intensified.
- Temperature field and thermal layer structure exhibited a descending trend for uplifting values of heat sink parameter.
- The N_t and N_b revealed opposite effect on the nanofluid concentration.
- The heat transfer rate at wall diminished with both fitted rate constant m and chemical reaction rate σ.
- Nanoparticle concentration was built up when activation energy parameter for chemical mechanism rises. Furthermore, impact of σ was qualitatively contradictory to that of E.

Acknowledgements This project was funded by the Deanship of Scientific Research (DSR) at King Abdulaziz University, Jeddah, under grant no. (RG-8-130-38). The authors, therefore, acknowledge with thanks the DSR's technical and financial support.

References

1. Choi, S.U.S.: Enhancing thermal conductivity of fluids with nanoparticles, p. 231. ASME, FED (1995)
2. Oztop, H.F.; Abu-Nada, E.: Numerical study of natural convection in partially heated rectangular enclosures filled with nanofluids. Int. J. Heat Fluid Flow **29**, 1326–1336 (2008)
3. Khan, W.A.; Khan, M.; Malik, R.: Three-dimensional flow of an Oldroyd-B nanofluid towards stretching surface with heat generation/absorption. PLoS ONE **9**(8), e10510 (2014)
4. Sheikholeslami, M.; Ellahi, R.: Three-dimensional mesoscopic simulation of magnetic field effect on natural convection of nanofluid. Int. J. Heat Mass Transf. **89**, 799–808 (2015)
5. Akbar, N.S.; Raza, M.; Ellahi, R.: Influence of induced magnetic field and heat flux with the suspension of carbon nanotubes for the peristaltic flow in a permeable channel. J. Mag. Mag. Mat. **381**, 405–415 (2015)
6. Sandeep, N.; Kumar, B.R.; Kumar, M.S.J.: A comparative study of convective heat and mass transfer in non-Newtonian nanofluid flow past a permeable stretching sheet. J. Mol. Liq. **212**, 585–591 (2015)
7. Rehman, S.; ul Haq, R.; Khan, Z.H.; Lee, C.: Entropy generation analysis for non-Newtonian nanofluid with zero normal flux of nanoparticles at the stretching surface. J. Taiwan Inst. Chem. Eng. **63**, 226–235 (2016)
8. Haq, R.; Khan, Z.H.; Hussain, S.T.; Hammouch, Z.: Flow and heat transfer analysis of water and ethylene glycol-based Cu nanoparticles between two parallel disks with suction/injection effects. J. Mol. Liq. **221**, 298–304 (2016)
9. Rahman, S.U.; Ellahi, R.; Nadeem, S.; Zia, Q.M.Z.: Simultaneous effects of nanoparticles and slip on Jeffrey fluid through tapered artery with mild stenosis. J. Mol. Liq. **218**, 484–493 (2016)
10. Hayat, T.; Rashid, M.; Imtiaz, M.; Alsaedi, A.: Nanofluid flow due to rotating disk with variable thickness and homogeneous–

heterogeneous reactions. Int. J. Heat Mass Transf. **113**, 96–105 (2017)
11. Hayat, T.; Javed, M.; Imtiaz, M.; Alsaedi, A.: Double stratification in the MHD flow of a nanofluid due to a rotating disk with variable thickness. Eur. Phys. J. Plus **132**, 146 (2017). https://doi.org/10.1140/epjp/i2017-11408-x
12. Sandeep, N.: Effect of aligned magnetic field on liquid thin film flow of magnetic-nanofluids embedded with graphene nanoparticles. Adv. Powder. Technol. **28**, 865–875 (2017)
13. Ramzan, M.; Ullah, N.; Chung, J.D.; Lu, D.; Farooq, U.: Buoyancy effects on the radiative magneto Micropolar nanofluid flow with double stratification, activation energy and binary chemical reaction. Sci Rep. **7**(12901), 12901 (2017). https://doi.org/10.1038/s41598-017-13140-6
14. Ramzan, M.; Bilal, M.; Chung, J.D.: Radiative flow of Powell–Eyring magneto-nanofluid over a stretching cylinder with chemical reaction and double stratification near a stagnation point. PLoS ONE **12**(1), e0170790 (2016)
15. Shafique, Z.; Mustafa, M.; Mushtaq, A.: Boundary layer flow of Maxwell fluid in rotating frame with binary chemical reaction and activation energy. Results Phys. **6**, 627–633 (2016)
16. Khan, W.A.; Alshomrani, A.S.; Khan, M.: Assessment on characteristics of heterogeneous-homogeneous processes in three-dimensional flow of Burgers fluid. Results Phys. **6**, 772–779 (2016)
17. Khan, W.A.; Irfan, M.; Khan, M.; Alshomrani, A.S.; Alzahrani, A.K.; Alghamdi, M.S.: Impact of chemical processes on magneto nanoparticle for the generalized Burgers fluid. J. Mol. Liq. **234**, 201–208 (2017)
18. Mustafa, M.; Khan, J.A.; Hayat, T.; Alsaedi, A.: Buoyancy effects on the MHD nanofluid flow past a vertical surface with chemical reaction and activation energy. Int. J. Heat Mass Transf. **108**, 1340–1346 (2017)
19. Khan, M.; Irfan, M.; Khan, W.A.: Impact of nonlinear thermal radiation and gyrotactic microorganisms on the magneto-Burgers nanofluid. Int. J. Mech. Sci. **130**, 375–382 (2017)
20. Ali, F.; Sheikh, N.A.; Saqib, M.; Khan, A.: Hidden phenomena of an MHD unsteady flow in porous medium with heat transfer. Nonlinear Sci. Lett. A **8**(1), 101–116 (2017)
21. Bhatti, M.M.; Zeeshan, A.; Ellahi, R.: Heat transfer with thermal radiation on MHD particle-fluid suspension induced by metachronal wave. Pramana J. Phys. **89**(3), 48 (2017). https://doi.org/10.1007/s12043-017-1444-6
22. Khan, M.; Ahmad, L.; Khan, W.A.: Numerically framing the impact of radiation on magneto-nanoparticle for 3D Sisko fluid flow. J. Braz. Soc. Mech. Sci. Eng. **39**, 4475–4487 (2017)